

Cite this: *Chem. Sci.*, 2019, 10, 4209

All publication charges for this article have been paid for by the Royal Society of Chemistry

## Dual-wavelength efficient two-photon photorelease of glycine by $\pi$ -extended dipolar coumarins†

Maxime Klausen,\* Victor Dubois, Guillaume Clermont, Claire Tonnelé, Frédéric Castet and Mireille Blanchard-Desce

Received 10th January 2019

Accepted 2nd March 2019

DOI: 10.1039/c9sc00148d

rsc.li/chemical-science

Photolabile protecting groups (PPGs) releasing bioactive compounds upon two-photon excitation have emerged as increasingly popular tools to control and study physiological processes. Yet the limited two-photon photosensitivity of many cages is still a critical issue for applications. We herein report the design, synthesis and photophysical study of polarized extended coumarinyl derivatives which show large two-photon sensitivity (up to 440 GM) at two complementary wavelengths in the NIR spectral range. DFT calculations demonstrate that subtle tuning of polarization in the ground-state and confinement of the photo-induced intramolecular charge transfer upon excitation is responsible for enhancing two-photon absorption while maintaining large uncaging efficiency. These findings open a new engineering route towards efficient coumarinyl PPGs.

### Introduction

Among the light-responsive organic structures available, uncagers<sup>1–3</sup> represent key tools for biological and biomedical studies. These compounds act as photolabile protecting groups (PPGs) towards bioactive messengers, drugs<sup>4–6</sup> or neurotransmitters,<sup>7–9</sup> by masking their biological function. Suitable light irradiation then triggers the physiological response by releasing the free molecule with remarkable temporal and spatial control. In this respect, two-photon excitation (2PE) with near infrared (NIR) light provides significant advantages.<sup>10–14</sup> As opposed to UV-visible light, NIR wavelengths allow deeper penetration in tissues, reduced photo-damage and intrinsic 3D resolution.<sup>10–14</sup> The photolytic efficiency of a cage upon 2PE is quantified by its two-photon uncaging (2PU) cross-sections  $\delta_u$  defined as  $\delta_u = \sigma_2 \Phi_u$ ; where  $\sigma_2$  is the two-photon absorption (2PA) cross-section (in GM) and  $\Phi_u$  the uncaging quantum yield.<sup>15</sup>

Until recently, the use of most cages described in the literature was somewhat limited for *in vivo* applications due to their low 2PU cross-sections (with  $\delta_u^{\text{max}}$  values below 1 GM).<sup>1,15</sup> To overcome this limitation and avoid the use of deleterious excitation powers, two main engineering strategies have been developed in the last decade: the modification of the  $\pi$ -conjugated backbone of known cages<sup>16–18</sup> or the design of 2P sensitized tandem systems.<sup>19,20</sup> Both strategies led in several cases to

innovative PPGs with  $\delta_u$  values over a dozen GM. In addition, the recent design of spectrally orthogonal cages is also of major promise for applications in neurosciences.<sup>21,22</sup> In this regard, we have been interested in the design of cages with two complementary activation wavelengths, able to photorelease key amino-acids both at 700 nm and at 900 nm. Such cages would profitably complement the photochemical toolbox for neuroscientists. In particular, glycine (Gly) plays an important co-agonistic role, along with glutamate, in NMDA extrasynaptic receptors and is thus a key inhibitor neurotransmitter.<sup>23</sup>

This motivated our effort towards the design of versatile and efficient Gly PPGs with very large 2P sensitivity (*i.e.* over 100 GM) at these two main working wavelengths where efficient uncaging of agonist (Glu) or antagonist (GABA) was previously accomplished.<sup>21</sup>

Among the variety of structures available, coumarinylmethyl PPGs are among the most widely studied molecular architectures.<sup>1,24</sup> The coumarin heterocyclic backbone, recognized as an efficient caging group,<sup>9,24–26</sup> can undergo a wide panel of chemical functionalization modulating its optical properties. Introducing an electron-withdrawing group (EWG) at the 3-position of the coumarin cage<sup>21,27,28</sup> was shown an influential way to red-shift both 1P and 2PA maxima respectively to the visible and the NIR,<sup>27,29–31</sup> as evidenced by **DEAC450** (Fig. 1).<sup>21</sup> Indeed, the design of **DEAC450**, which allows the photorelease of caged acids (Glu, GABA) with blue light irradiation (instead of UV irradiation for seminal compound DEAC) or upon 2P excitation at 900 nm, was a crucial step forward in the development of efficient cages of interest for neuroscientists. In addition, **DEAC450** was demonstrated to show a very good uncaging quantum yield for glutamate release (39%), while DEAC had an uncaging quantum yield of

Univ. Bordeaux, Institut des Sciences Moléculaires (UMR5255 CNRS), 351 cours de la Libération, F-33405, Talence, France. E-mail: mireille.blanchard-desce@u-bordeaux.fr

† Electronic supplementary information (ESI) available: Experimental details of synthesis, photophysical and photochemical studies. DFT calculations. See DOI: 10.1039/c9sc00148d





Fig. 1 Recent evolution in the structure of  $\pi$ -extended coumarin PPGs and structures designed in the present work.

12%. This demonstrated that the extension of the coumarinyl moiety at the 3-position could indeed shift the absorption spectra towards the visible but also significantly affect the photolysis efficiency. Yet, albeit causing a substantial increase of uncaging quantum yield for amino-acid release, the acrylamide extension implemented in DEAC450 appeared to have limited effects on its 2PA properties, as indicated by the reported  $\delta_{\text{u}}$  value (0.5 GM at 900 nm in physiological conditions).<sup>21</sup> This consideration led us to build our strategy on the increase of the 2PA response in new D- $\pi$ -A extended DEAC derivatives, by (i) modulating the intramolecular charge transfer in the ground-state to achieve optimum polarization leading to maximal 2PA<sup>32</sup> and (ii) further extending the  $\pi$ -conjugated system (Fig. 1). A major questioning was to assess how the photochemistry of the original cage is affected by such changes, and to determine to what extent the electronic distribution of the PPG can be tuned in order to maximize the  $\sigma_2$  without impeding the photolytic process. We thus prepared a small library of extended dipolar coumarinylmethyl derivatives bearing dedicated electron-withdrawing end-groups (EWG) at the 3-position (Fig. 1). To fulfil this role, we chose nitrogen-based aromatic heterocycles such as thiazoles and derivatives<sup>33</sup> (Fig. 1). These new PPGs were then used to cage and release Fmoc-protected glycine with two primary goals: (i) performing a model study of the parameters regulating their photolytic efficiency, and (ii) enlightening the experimental results with DFT calculations in pursuance of rationale in the design of such coumarinyl PPGs.

## Results and discussion

### Design and synthesis

The synthetic layout of the new “free” DEAC cages involves three main challenges: the introduction of the fundamental 4-

hydroxymethyl group on the aminocoumarin skeleton, the synthesis of the vinyl-acceptor moiety, and finally functionalization at the 3-position with the double bond. The formation of the alcohol **1** was achieved starting from the commercially available 7-diethylamino-4-methylcoumarin using an original pathway involving the formation of an intermediate enamine<sup>34</sup> which was found to be much cleaner, more efficient and convenient than the usual selenium dioxide oxidation<sup>35</sup> in our hands (Scheme S1†). The extension of the  $\pi$ -conjugated system at the 3-position of the coumarin scaffold was then achieved by Heck cross-coupling using the iodinated substrate **2**.

Iodination of the free alcohol **1** was successfully performed in good yield and large scale by using *N*-iodosuccinimide in the presence of a strong Lewis acid, which provided a highly activated source of electrophilic iodine (Scheme 1).

The vinyl-based electron-accepting modules were synthesized by different procedures, depending on the synthon. 2-Vinylbenzothiazole, -benzoxazole, and -benzothiadiazole derivatives (**4**, **5** and **6**) were synthesized by Suzuki coupling with potassium vinyl trifluoroborate.<sup>36,37</sup> 2-Vinylthiazole (**3**) and 9,9-dibutyl-7-vinyl-9H-fluorene-2-carbaldehyde (**7**) were obtained by Wittig reactions starting from the corresponding aldehydes (see ESI†). Heck reaction using Jeffery conditions<sup>21,38</sup> between intermediates **2** and **3–7** finally afforded compounds **8–12** in good to excellent yields, often without extensive purification (Scheme 1).

Eventually, condensation of intermediate **12** with 2-aminothiophenol hydrochloride yielded without additional protection step a fluorene-containing derivative **18**, which was then esterified with Fmoc-Gly-OH to yield the final PPG **19** (Scheme 2).

### Photophysical properties

With all compounds in hands, the photophysical one- and two-photon absorption properties were investigated. Dimethylsulfoxide was chosen as solvent for the photophysical study due to its high polarity (thus closer to water than low-polarity organic solvents) reasonable viscosity (favourable to fluorescence) and optimal solubility of the whole series of compounds.

All new PPGs show intense absorption in the visible and fluorescence properties (see spectra in ESI†). Experimental data are summarized in Table 1. As expected, the extension of the  $\pi$ -conjugated system with a vinyl-acceptor group at the 3-position induced a marked bathochromic and hyperchromic shift in absorption and red-shifted emission as compared to DEAC. This trend is amplified by the addition of the fused benzenic ring in the heterocyclic end-group, responsible for an additional 13 to 28 nm red-shift of the absorption band from thiazole to benzothiadiazole compared to DEAC450. A significant hyperchromic effect is also observed, as supported by the 40% enhancement of the  $\epsilon^{\text{max}}$  value in **14** compared to DEAC450. Interestingly, the elongated fluorenyl compounds **17** and **19** showed an intermediary behaviour, with absorption coefficients falling in the same range as the vinyl derivatives **14** and **15** but with less marked bathochromic shifts of their absorption/emission compared to DEAC450. Among the series, compound **16** which bears the strongest EWG shows a singular





Scheme 1 Synthesis of extended polarized coumarin cages. Reagents and conditions: (a) NIS,  $\text{BF}_3 \cdot \text{Et}_2\text{O}$ ,  $\text{CHCl}_3$ , 0 °C to r.t. (70%). (b) **3**–**7**,  $\text{Pd}(\text{OAc})_2$ ,  $n\text{-Bu}_4\text{NCl}$ , LiCl,  $\text{NaHCO}_3$ , DMF, 130 °C (**8**, 90%; **9**, 96%; **10**, 92%; **11**, 76%; **12**, 89%). (c) Fmoc-Gly-OH, EDC·HCl, DMAP (cat.),  $\text{CH}_2\text{Cl}_2$ , r.t. (**13**, 52%; **14**, 59%; **15**, 69%; **16**, 58%; **17**, 84%).



Scheme 2 Synthesis of cage **19**. Reagents and conditions: (a) 2-aminothiophenol hydrochloride, DMF, 120 °C (42%). (b) Fmoc-Gly-OH, EDC·HCl, DMAP (cat.), (64%).

behaviour, with an absence of hyperchromic effect but a marked red-shifted and much weaker emission compared to **DEAC450**. This suggests that strong photo-induced ICT takes place after excitation prior to emission. This leads to a strongly polarized emissive excited-state which is stabilized by polar environments. This is confirmed by the pronounced positive fluorescent solvatochromic behaviour of this compound, not observed in other derivatives (see ESI<sup>†</sup>), and further demonstrated by DFT calculations (*vide infra*).

### Uncaging properties

One-photon uncaging efficiencies were then assessed by irradiating samples of the new compounds and reference PPG at 455 nm, and monitoring unambiguously the release rate of the caged Fmoc-Gly-OH upon irradiation by <sup>1</sup>H NMR (Fig. 2a). For the sake of comparison, we performed the photolysis in a  $\text{CD}_3\text{CN}/\text{D}_2\text{O}$  (9/1, v/v) mixture which is commonly used in the literature.<sup>27,39–41</sup> In this model study, we also decided to preserve

the protecting group on the glycine ester, which quite conveniently allowed the quantitation of the released species (rather than degradation of the cage) either by monitoring the  $\text{CH}_2$  of the amino-acid itself or that of the Fmoc protecting group.

First order kinetics were observed in all cases (Fig. 2b), allowing the derivation of the one-photon uncaging sensitivity  $\epsilon_{455} Q_u^{\text{rel}}$  from the slope values compared to those of **DEAC450-Gly** irradiated in the exact same conditions (see ESI<sup>†</sup>),<sup>42</sup> and subsequently, the ratio of the relative uncaging quantum yield  $Q_u^{\text{rel}}$  value toward the reference uncaging quantum yield  $\Phi_u^{\text{ref}}$  (Table 2).

All compounds except **19** proved to have lesser uncaging rates than **DEAC450-Gly**. Yet, the relative uncaging quantum yields still reached 20% for compound **13**, which remains higher than most PPGs described so far. A marked reduction of the  $Q_u^{\text{rel}}$  value was revealed by benzo-compounds **14** and **15** whose efficacy is largely reduced (by about 50% compared to compound **13**) indicating that the presence of the fused ring on the EWG is detrimental to the photorelease efficiency. Most markedly, compound **16** did not proceed to uncaging of glycine upon excitation, and proved unsuitable for uncaging applications.

The benzothiadiazolyl end-group, the strongest EWG in the series, is clearly detrimental to photolysis, indicating that a strongly polarized excited-state and marked photo-induced ICT is unfavourable for this specific purpose. This behaviour was further confirmed by DFT calculations, which revealed that the elongation of the C–O bond upon excitation in compound **16** is 2–3 times smaller than in the other compounds (*vide infra*).

Surprisingly, a different behaviour was observed for extended derivatives **17** and **19** bearing a fluorenyl unit in the conjugated  $\pi$ -connector. While the aldehyde derivative **17** displays a moderate but still reasonable  $Q_u^{\text{rel}}$  of 9%, the



Table 1 Photophysical (1P and 2P) properties of **13–17**, **19** and reference compound **DEAC450** in DMSO

Cpd	$\lambda_{\text{abs}}^{\text{max}}$ (nm)	$\epsilon^{\text{max}}$ ( $\text{M}^{-1} \text{cm}^{-1}$ )	$\lambda_{\text{em}}^{\text{max}}$ (nm)	$\Phi_{\text{f}}$	$\lambda_{2\text{PA}}^{\text{max}}$ (nm)	$\sigma_2^{\text{maxc}}$ (GM)
<b>DEAC450</b>	444	$3.4 \times 10^4$	523	0.82 <sup>a</sup>	890	123
<b>13</b>	457	$3.6 \times 10^4$	541	0.95 <sup>a</sup>	950	164
					700	191
<b>14</b>	472	$4.7 \times 10^4$	562	0.87 <sup>a</sup>	970	371
					710	441
<b>15</b>	467	$4.6 \times 10^4$	552	0.92 <sup>a</sup>	970	267
					700	367
<b>16<sup>d</sup></b>	472	$3.3 \times 10^4$	692	0.13 <sup>b</sup>	970	215
					730	191
<b>17</b>	457	$4.6 \times 10^4$	553	0.56 <sup>a</sup>	940	147
					730	621
<b>19</b>	458	$4.2 \times 10^4$	547	0.59 <sup>a</sup>	940	143
					730	988

<sup>a</sup> Fluorescence quantum yield (standard: fluorescein in 0.1 M NaOH ( $\Phi_{\text{f}} = 0.9$ )). <sup>b</sup> Fluorescence quantum yield (standard: rhodamine 6G in EtOH ( $\Phi_{\text{f}} = 0.94$ )). <sup>c</sup> 2PA cross-section at  $\lambda_{2\text{PA}}^{\text{max}}$  derived from 2PEF experiments in DMSO. <sup>d</sup> 2PA measurement performed in toluene.

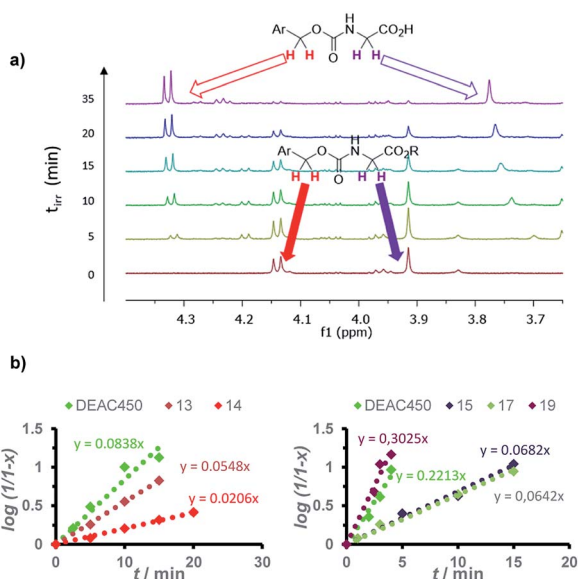


Fig. 2 (a) Example of evolution of the  $^1\text{H}$  NMR spectrum of the coumarinyl PPG **14** upon excitation at 455 nm in  $\text{CD}_3\text{CN}/\text{D}_2\text{O}$  (9/1, v/v), and kinetic follow-up of the photorelease. (b) Comparative kinetics of photolysis upon irradiation at 455 nm of the reference PPG (**DEAC450**) and new polarized PPGs in  $\text{CD}_3\text{CN}/\text{D}_2\text{O}$  at 0.7 mM (left) or at 0.25 mM (right); derived from  $^1\text{H}$  NMR experiments.

benzothiazolyl derivative **19** shows an uncaging efficiency comparable to that of **DEAC450** (Table 2). Indeed, **19** proved slightly faster than reference compound **DEAC450** upon 1P photolysis, leading to a  $Q_{\text{u}}^{\text{rel}}$  value of 45%, whereas its vinyl counterpart **14** displayed a  $Q_{\text{u}}^{\text{rel}}$  value of only 8%. This suggests that the introduction of an intermediate fluorenyl  $\pi$ -bridge in compound **19** is responsible for a redistribution in the electron density,<sup>43</sup> favouring significant increase of  $\Phi_{\text{u}}$ .

### Dark stability

Importantly, whereas amino acid esters have sometimes been reported unstable in aqueous media,<sup>9</sup> all of our new compounds

proved to be stable towards dark hydrolysis in this photolysis medium, as no significant degradation of the chromophores was observed after several days in solution in the dark at room temperature (see ESI<sup>†</sup>).

### DFT calculations

DFT calculations conducted at the M06-2X/6-311G(d) level<sup>44</sup> were performed to gain further insight into the polarization and electronic structures of the ground and first excited states of these derivatives. Table 3 reports the vertical spectroscopic properties of the investigated compounds, together with the electric dipoles of the  $S_0$  and  $S_1$  states ( $\mu_0$  and  $\mu_1^{\text{vert}}$ ) and their difference ( $\Delta\mu_{01}^{\text{vert}}$ ). The computed absorption spectra are reported in ESI<sup>†</sup>. In every compound, the first optically allowed excited state ( $S_1$ ) is dominated by a HOMO  $\rightarrow$  LUMO  $\pi$ - $\pi^*$  excitation. Excitations implying the HOMO-1 and LUMO+1 also contribute to the  $S_0 \rightarrow S_1$  transition in extended derivatives **17** and **19** (see ESI<sup>†</sup> for details). The isodensity surfaces of the frontier orbitals are sketched in Fig. 3 and show that both HOMO and LUMO are delocalized along the conjugated part of the molecule.

As shown in Table 3, TDDFT calculations qualitatively reproduce the red-shifts measured experimentally upon substitution at the 3-position of the coumarin cage. With respect to the reference compound **DEAC450**, adding a fused benzenic ring on the terminal EWG (from thiazole in compound **13**, to benzothiazole in compound **14**) results in computed bathochromic shifts of 0.08 and 0.17 eV, respectively, which compares well with the measured bathochromic displacements of 0.19 and 0.25 eV. Besides, the associated increase of the oscillator strength is also in accordance with the hyperchromic shift observed experimentally. The absence of further red-shift of the absorption band in the more extended compounds **17** and **19** is similarly well reproduced. Finally, TDDFT calculations support the specific spectroscopic properties of compound **16**, which shows a marked bathochromic but no significant hyperchromic shift with respect to **DEAC450**. These spectral evolutions can be traced back to the magnitude of the photo-



Table 2 Photochemical (1P and 2P) properties of **13–17**, **19** and reference compound **DEAC450** in aqueous acetonitrile

Cpd	$\epsilon_{455 \text{ nm}} (\text{M}^{-1} \text{cm}^{-1})$	$Q_u^{\text{rel}}/\Phi_u^{\text{ref}}$	$Q_u^{\text{relb}}$	$\epsilon_u^{\text{maxc}} (\text{M}^{-1} \text{cm}^{-1})$	$\lambda_{2\text{PA}}^{\text{max}} (\text{nm})$	$\delta_u^{\text{maxd}} (\text{GM})$
<b>DEAC450</b>	$3.2 \times 10^4$	1	0.39	$13 \times 10^3$	890	48
<b>13</b>	$3.6 \times 10^4$	0.50	0.20	$7.8 \times 10^3$	950	32
					700	37
<b>14</b>	$4.1 \times 10^4$	0.21	0.08	$4.0 \times 10^3$	970	30
					710	36
<b>15</b>	$4.1 \times 10^4$	0.24	0.09	$4.5 \times 10^3$	970	25
					700	35
<b>16</b>	$3.0 \times 10^4$	<0.02	—	—	970	—
					730	—
<b>17</b>	$4.6 \times 10^4$	0.23	0.09	$4.2 \times 10^3$	940	13
					730	56
<b>19</b>	$4.3 \times 10^4$	1.14	0.45	$21 \times 10^3$	940	64
					730	442

<sup>a</sup> Ratio of uncaging quantum yield values derived from comparative 1P photolysis experiments in  $\text{CD}_3\text{CN}/\text{D}_2\text{O}$  (9/1, v/v) at 455 nm. <sup>b</sup> Uncaging quantum yield values calculated using  $\Phi_u^{\text{ref}} = 0.39$  for **DEAC450**[Gly]. <sup>c</sup> One-photon uncaging sensitivity at  $\lambda^{\text{max}}$ . <sup>d</sup> Two-photon uncaging sensitivity at  $\lambda_{2\text{PA}}^{\text{max}}$  estimated from comparative 1P photolysis experiments and 2PEF measurements.

Table 3 Vertical transition energy ( $\Delta E_{01}$ , eV) and wavelength ( $\lambda_{01}$ , nm), as well as, oscillator strength ( $f_{01}$ ), transition dipole moment ( $\mu_{01}$ , D), ground state and excited state dipole moments ( $\mu_0$  and  $\mu_1^{\text{vert}}$ , D), dipole moment variation ( $\Delta\mu_{01}^{\text{vert}}$ , D), charge transferred upon excitation ( $q^{\text{CT}}$ , |e|), and charge transfer distance ( $d^{\text{CT}}$ , Å), calculated at the TDDFT/M06-2X/6-311G(d) level in acetonitrile

Cpd	$\lambda_{\text{exp}}$	$\Delta E_{\text{exp}}$	$\Delta E_{01}$	$\lambda_{01}$	$f_{01}$	$\mu_{01}$	$\mu_0$	$\mu_1^{\text{vert}}$	$\Delta\mu_{01}^{\text{vert}}$	$q^{\text{CT}}$	$d^{\text{CT}}$
<b>DEAC450</b>	444	2.793	3.125	397	1.39	10.81	6.76	14.99	8.25	0.584	2.940
<b>13</b>	457	2.713	2.935	422	1.70	12.36	6.38	12.41	6.70	0.540	2.581
<b>14</b>	472	2.627	2.874	431	1.87	13.09	7.52	14.89	8.09	0.568	2.967
<b>15</b>	467	2.655	2.902	427	1.84	12.94	8.05	14.97	7.59	0.566	2.789
<b>16</b>	472	2.627	2.941	422	1.55	11.78	12.92	22.51	10.53	0.581	3.775
<b>17</b>	457	2.713	3.012	412	2.23	13.99	14.39	21.28	7.18	0.551	2.714
<b>19</b>	458	2.707	3.004	413	2.57	15.02	11.22	17.10	6.35	0.544	2.433

induced ICT, which is quantified by the dipole moment variation  $\Delta\mu_{01}^{\text{vert}}$ . In particular, the largest  $\Delta\mu_{01}^{\text{vert}}$  value is found for **16**, which is mostly related to an increased charge transfer distance  $d^{\text{CT}}$  in this compound. The total charge transferred is however of similar magnitude for all compounds (Table 3).

In order to gain better insight into the difference of photochemical behavior between derivatives, relaxed geometries of the  $S_1$  states were calculated. Table 4 reports the photo-induced elongation of the C–O single bond connecting the glycine ester to the coumarinylmethyl protecting moiety, defined as the difference between the C–O distances issued from  $S_1$  and  $S_0$  gas phase optimizations ( $\Delta_{\text{CO}} = d_{\text{CO}}^{S_1} - d_{\text{CO}}^{S_0}$ ). The adiabatic ( $E_{\text{adia}}$ ) and 0–0 energies ( $E_{0-0}$ ) are also reported, as well as the excited-state dipole moment ( $\mu_1^{\text{opt}}$ ) and photo-induced dipole moment variation ( $\Delta\mu_{01}^{\text{opt}}$ ) calculated using relaxed gas phase geometries ( $\Delta\mu_{01}^{\text{opt}} = \mu_1^{\text{opt}} - \mu_0$ ). Finally, these last two quantities were further refined to account for solvent effects, by performing IEF-PCM:TD-DFT single-point calculations (Table 4, last columns).

We note a slight elongation of the C–O bond in all compounds in relaxed excited state  $S_1$  from which photochemistry and fluorescence occur. It is interesting to note that compound **16** exhibits the smallest  $\Delta_{\text{CO}}$  value within the series (more than twice smaller than that of **DEAC450**), together with the largest excited-state dipole moment ( $\mu_1^{\text{opt+ts}} = 23$  D, about

twice larger than that of **DEAC450**), and photo-induced dipole moment variation. This result confirms that the large photo-induced ICT occurring within this compound is detrimental to its uncaging efficiency. On the other hand, all other new derivatives (**13–15**, **17**, **19**) show similar  $\Delta_{\text{CO}}$  values, close to that of **DEAC450**.

Neither the excited dipole moments values, nor the variation of dipole moment appear to show direct correlation with uncaging efficiency. However, closer examination of HOMO–LUMO<sup>43</sup> does reveal interesting features. For compounds **13–16**, photo-induced ICT extends to the EW end-groups; the sharpest effect being observed for compound **16** which bears the strongest terminal EWG. In contrast, the photo-induced ICT remains mostly limited to the extended conjugated system in compound **17** and **19**. Furthermore, comparison of the  $d^{\text{CT}}$  values of these two compounds (Table 3) indicates that extension of the photo-induced ICT leads to a decrease of uncaging efficiency (Fig. 4).

To further investigate the origin of difference in uncaging efficiency between derivatives **13–17**, and **19**, calculation of the carbocations that are presumed key intermediates in the photolysis mechanism<sup>45,46</sup> was undertaken (see ESI†). Starting from the relaxed geometries of the  $S_1$  photo-activated state, rigid energy scans were first performed by elongating progressively the C–O bond up to the photolytic dissociation limit, in





Fig. 3 Graphical representations of the frontier orbitals of the investigated compounds, calculated at the IEFPCM:M06-2X/6-311G(d) level.

Table 4 Photo-induced elongation of the C–O bond ( $\Delta_{CO}$ , Å), adiabatic ( $E_{\text{adia}}$ , eV) and 0–0 energies ( $E_{0-0}$ , eV), excited state dipole moment ( $\mu_1^{\text{opt}}$ , D) and dipole moment variation ( $\Delta\mu_{01}^{\text{opt}}$ , D), obtained from the gas phase geometries of the  $S_1$  and  $S_0$  states both optimized at the M06-2X/6-311G(d) level

	Gas					Acetonitrile	
	$\Delta_{CO}$	$E_{\text{adia}}$	$E_{0-0}$	$\mu_1^{\text{opt}}$	$\Delta\mu_{01}^{\text{opt}}$	$\mu_1^{\text{opt+s}}$	$\Delta\mu_{01}^{\text{opt+s}}$
<b>DEAC450</b>	0.018	3.309	3.221	9.11	4.27	13.97	7.26
<b>13</b>	0.015	3.061	2.987	6.85	2.60	11.05	5.37
<b>14</b>	0.013	2.983	2.909	8.19	2.95	13.79	6.98
<b>15</b>	0.014	3.021	2.944	7.75	2.23	13.60	6.23
<b>16</b>	0.008	2.895	2.828	15.13	5.90	22.99	10.99
<b>17</b>	0.015	2.971	2.907	13.37	2.85	20.48	6.97
<b>19</b>	0.014	2.928	2.863	9.80	2.61	16.35	6.53

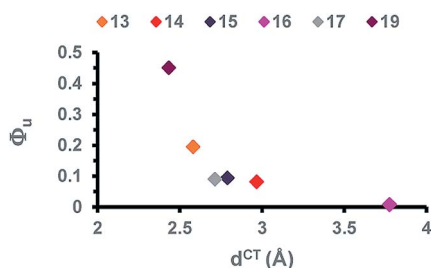


Fig. 4 Correlation between the extent of photo-induced ICT ( $d^{\text{CT}}$ ) and the relative uncaging quantum yields  $\Phi_u^{\text{rel}}$  in compounds 13–17 and 19.

order to evaluate the bond dissociation energy (BDE) in the excited electronic state. Geometry optimizations of the carbocations were also conducted in the  $S_0$  state to compare their relative stability with respect to the parent coumarinyl

derivatives (see ESI<sup>†</sup>). These two series of calculations led to very similar conclusions. Interestingly, fluorenyl-based compounds 17 and 19 give rise to the lowest BDE and to the most stable carbocations within the series whereas compounds 14 and 15 lead to the largest BDE and to the least stable carbocations. We note however that the compound **DEAC450** falls out of the correlation (as was the case for  $d^{\text{CT}}$ ) suggesting that different mechanisms might be involved.

### Two-photon absorption

The two-photon absorption spectra of the new PPGs 13–17 and 19 were determined by conducting two-photon excited fluorescence experiments (2PEF) in DMSO solution (Table 1). DMSO was chosen as a viscous non-protic solvent, thus promoting fluorescence (Table 1) and allowing accurate and reliable 2PA measurements. At opposite, the presence of water, although beneficial to photorelease, logically reduces fluorescence.

All compounds exhibit *two intense 2PA bands* in the spectral range of interest (690–1000 nm) which is not the case of **DEAC450** (Fig. 5a and b) which is blue-shifted compared to the series of compounds investigated.

An intense band located at about twice the maximum wavelength of 1PA (see ESI<sup>†</sup>) is observed around 940–970 nm with maximum 2PA cross-sections varying between 140 and 370 GM. Firstly, we note that the maximum 2PA cross-section measured for **DEAC450** in DMSO (123 GM at 890 nm) is almost two orders of magnitude larger than the one derived from  $\delta_u$  and  $\Phi_u$  values reported in buffered water (*i.e.*, 1.3 GM). This difference may partly be related to solvent effect as water may significantly affect 2PA. We note that 2PA measurements reported earlier for coumarin 1, a 4-methyl analogue of DEAC yielded a maximum 2PA cross-section in ethanol of 103 GM at 755 nm.<sup>47</sup> Our measurements gave a  $\sigma_2^{\text{max}}$  value of 44 GM at



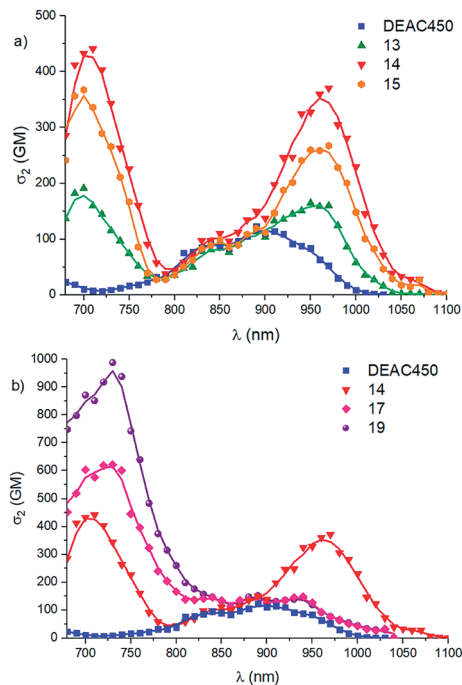


Fig. 5 Comparison of the 2PA spectra of (a) vinyl derivatives 13–15 and DEAC450 in DMSO; (b) dipolar compounds 14, 17, 19 and DEAC450 in DMSO.

760 nm for DEAC450 in DMSO (see ESI†), illustrating the influence of the environment and electric field effects on 2PA. These values are consistent with the larger maximum 2PA cross-section measured for extended DEAC450 at 890 nm (123 GM). The almost two-orders of magnitude smaller  $\sigma_2^{\max}$  value derived from the reported  $\delta_u$  value (1.3 GM) suggests that formation of dimers of DEAC450 may occur in the aqueous environment where  $\delta_u$  measurements were conducted. Indeed formation of dimers of dipolar chromophores may significantly reduce 2PA properties.<sup>48</sup>

Secondly, we observe that all new derivatives show red-shifted and more intense 2PA responses than DEAC450 (Fig. 5). While compound 13 shows slightly larger  $\sigma_2^{\max1}$  value (165 GM instead of 123 GM) than DEAC450, the additional fused benzenic ring on the EWG in 14 and 15 induces a two to three fold enhancement of this value (*i.e.*, 370 GM and 270 GM respectively). In contrast, the  $\epsilon^{\max}$  values were found to increase by only 40%, evidencing stronger effect on 2PA. As a result, extended coumarin derivatives 14 and 15 show unprecedented 2PA responses at 970 nm, over one order of magnitude larger than coumarin fluorochromes commonly used in bioimaging.<sup>49</sup> We also note that compound 14 shows a 37% larger  $\sigma_2^{\max1}$  value as compared to compound 15, confirming that the benzothiazole EWG leads to larger 2PA responses than benzoxazole.

Compound 16, which bears the strongest EWG in the series and shows the largest polarization for derivatives of similar length (see Table 3,  $\mu_0 = 12.9$  D), shows a broader and weaker 2PA band than compounds 14 and 15, with a  $\sigma_2^{\max1}$  reaching 215 GM. This indicates that derivatives 14 and 15 are close to optimum polarization ( $\mu_g = 7.5$  and 8.0 D) leading to maximal

2PA, while compound 16 is most probably too polarized (*i.e.* over optimum ICT in the ground state).<sup>32</sup> In contrast, extended derivatives 17 and 19 show  $\sigma_2^{\max1}$  values which are similar and only slightly larger than that of DEAC450 (*i.e.* 150 and 140 GM). Hence the presence of the fluorenyl bridge is detrimental to the low energy 2PA band, in relation with lesser ICT in the ground state due to the higher cost associated with charge separation along the full length of molecules 17 and 19.<sup>32</sup>

Strikingly, a second and even more intense higher energy band is observed around 700–730 nm for all new PPGs (Fig. 5). This higher energy band is strongly 2P allowed and corresponds to a strongly 1P allowed excited-state only for extended compounds 17 and 19 (see ESI†). The addition of a fused benzenic ring in the terminal EWG induces a significant increase of the  $\sigma_2^{\max2}$  bands (Fig. 5a), as indicated by the comparison of compounds 13 and 14. The nature of the heterocyclic moiety, also significantly influences the  $\sigma_2^{\max2}$  values as witnessed by the 19% increase observed in the benzothiazole PPG 14 (440 GM) compared to its benzoxazole counterpart 15 (370 GM).

Again, compound 16 shows a different behaviour. Due to its far-red/NIR emission in DMSO, which prevented access to the higher energy band located around 700 nm by 2PEF measurements, 2PA measurements were conducted in toluene in which compound 16 emits in the visible, see ESI†). The resulting measurements in the full 700–1100 nm range do reveal a second high energy band, as in the other dipolar compounds. As was the case for the low-energy 2PA band, the  $\sigma_2^{\max2}$  value (around 200 GM, see Table 1) is again much lower than for analogues 14 and 15 of similar size.

In contrast, a spectacular influence of the fluorenyl bridge is evidenced in compounds 17 and 19 (Fig. 5b). Unlike their lower-energy 2PA bands, the transitions located at 730 nm show very high maxima, with a  $\sigma_2^{\max2}$  value twice larger for the benzothiazolyl derivative 19 than for its shorter analogue 14. With a remarkable  $\sigma_2^{\max}$  value of 990 GM, compound 19 also exhibits a 60% higher 2PA cross-section than its aldehyde counterpart 17, hereby evidencing the role of the EWG in the phenomenon. The differences in the 2PA higher energy maxima of these three compounds can be related to the nature of the second optically allowed absorption band, as rationalized by DFT calculations (see ESI†). In compound 19, the  $S_0 \rightarrow S_2$  transition is strongly optically allowed (as indicated by its large oscillator strength,  $f_{02} = 0.55$ ), and associated to a large photo-induced dipole variation ( $\Delta\mu_{02} = 6.89$  D). In compound 17, absorption towards the second bright excited state (which corresponds to the  $S_0 \rightarrow S_3$  transition) also gives rise to a significant reorganization of the electron density ( $\Delta\mu_{03} = 8.58$  D) but with a twice-smaller intensity ( $f_{03} = 0.29$ ). In 14, the intensity of the  $S_0 \rightarrow S_2$  transition is much weaker ( $f_{02} = 0.13$ ) and associated to a negligible  $\Delta\mu_{02}$  value (0.46 D).

## Two-photon uncaging

As discussed above, the nature of the EWGs as well as the presence of a conjugated linker significantly affects both the 2PA response and the uncaging efficiency. In particular optimum polarization leads to very large 2PA responses both at



970 nm (370 and 270 GM for compounds **14** and **15** respectively) and 700 nm (440 GM and 370 GM for compounds **14** and **15**) while insertion of the fluorenyl unit in the conjugated system leads to very large 2PA responses at 730 nm. Besides, the extension of electronic redistribution ( $d^{CT}$ ) is detrimental to the uncaging efficiency. Hence both tuning of ICT in the ground-state and limitation of electronic redistribution upon excitation are key parameters which control the two-photon sensitivity ( $\delta_u = \sigma_2 \times \Phi_u$ ).

Extrapolated 2P uncaging sensitivities derived from previous measurements of 2PA cross-section and uncaging quantum yield are reported in Table 2. Although the nature of solvent does affect the 2PA response (*vide supra*), these values give consistent trends among the series of derivatives and allow direct comparison with **DEAC450**. For PPGs of the vinyl series **13–15**, the increase in  $\sigma_2^{\max}$  is somewhat counterbalanced by a drop of  $Q_u^{\text{rel}}$ . Yet, in all three cases, the calculated  $\delta_u$  values reach about 35 GM for irradiation in the higher energy band and 25–30 GM for the lowest energy band. These values are only slightly smaller than that extrapolated for **DEAC450**,<sup>50</sup> their main advantage being that they can be used either at 700–720 nm (like DEAC or MNI)<sup>8,25</sup> or at 950 nm, thus offering improved penetration depth and interesting sequential alternatives for *in vivo* experiments. As such they represent promising uncaging tools to be used in conjunction with complementary cages that would photorelease antagonists and coagonists of Gly.

Eventually, thanks to its very large 2PA cross-sections in the 700–750 nm range (over 700 GM) combined with a slightly improved uncaging quantum yield with respect to **DEAC450**, the extended fluorenyl derivative **19** shows a record estimated  $\delta_u$  of about 440 GM at 730 nm. To confirm the potential use of this new derivative in 2P uncaging experiments, we performed the irradiation of **19** at both 2P maxima for 7 h in similar conditions, and compared the conversion of the photolysis reaction with two appropriate standards, *i.e.* DEAC at 730 nm and **DEAC450** at 940 nm (Fig. 6). Irradiation of the samples at 730 nm clearly evidenced a sevenfold enhancement in 2P photosensitivity between compound **19** and parent DEAC, in agreement with  $\delta_u$  values derived from 1P uncaging studies and 2PEF measurements using the  $\delta_u = \sigma_2 \times \Phi_u$  relationship. Furthermore, we observe a major enhancement (by about a factor 8) of the 2P sensitivity of compound **19** at 730 nm compared to its 2P photosensitivity at 940 nm. Again, this is consistent with the relative  $\delta_u$  values derived at 730 and 940 nm



Fig. 6 Comparative histogram showing the conversion of the uncaging reaction (Gly release) after 7 h of two-photon irradiation at 730 and 940 nm in similar conditions (1.2 mL, 1 W).

for this compound, thus validating our study. Finally, comparative irradiation of **DEAC450** and compound **19** at 940 nm indicate an enhancement of 2P sensitivity by over a factor 2, as anticipated from comparison of  $\delta_u$  values of both compounds derived from 1P uncaging and 2PEF studies.

This study demonstrates that by tuning ICT in the ground state and electronic redistribution in the photoactive excited state, we could indeed enhance both uncaging efficiency and 2PA properties. As a result, coumarin derivative **19** shows unprecedented 2P sensitivity at 730 nm while retaining similar 2P sensitivity at 890 nm as **DEAC450**. In contrast, shorter derivative **13** shows similar 2P sensitivity, comparable to **DEAC450**, at two complementary wavelengths (700 and 950 nm).

## Conclusion

This work unveils a new direction towards dipolar coumarin cages with unique two-photon uncaging sensitivity. The combination of experimental spectroscopic investigation with computational chemistry revealed surprising structure–property relationships where subtle tuning of the ground-state polarization and containment of photo-induced redistribution in the excited state triggers both the photolysis and the 2PA ability. These achievements open the route to unique opportunities in neurosciences. Further work along that direction is currently in progress.

## Computational methods

The geometry of the ground ( $S_0$ ) and first singlet excited ( $S_1$ ) states were optimized in the gas phase in the framework of the Density Functional Theory (DFT) using the M06-2X exchange–correlation functional<sup>44</sup> and the 6-311G(d) basis set. All structures were characterized as real minima of the potential energy surface on the basis on their positive vibrational force constants. Ground state optimized geometries were used to compute the vertical transition energies and excited state properties by employing the Time-Dependent Density Functional Theory (TD-DFT) at the M06-2X/6-311G(d) level. Solvent effects (acetonitrile) were taken into account in these calculations by using the Integral Equation Formalism of the Polarizable Continuum Model (IEF-PCM).<sup>51</sup> The photo-induced charge transfer was analyzed on the basis of vertical electronic transitions, by considering the difference  $\Delta\mu_{01}^{\text{vert}}$  in the electric dipoles of the  $S_0$  and  $S_1$  states. Using the approach reported in ref. 52 and 53,  $\Delta\mu_{01}^{\text{vert}}$  was further decomposed as  $\Delta\mu_{01}^{\text{vert}} = q^{\text{CT}} \times d^{\text{CT}}$ , where  $q^{\text{CT}}$  is the photo-induced charge transfer, *i.e.* the global amount of charge transferred upon light excitation, and  $d^{\text{CT}}$  is the distance over which this charge is transferred.

Then, the effects of structural relaxation on the electronic structure of the  $S_1$  state were addressed. The adiabatic energies, defined as the energy difference of the  $S_1$  and  $S_0$  states in their respective minimum ( $E_{\text{adia}} = E_{S_1}^{\text{opt}} - E_{S_0}^{\text{opt}}$ ), were calculated on the basis of the gas phase geometries. The 0–0 energies were then evaluated as the sum of the adiabatic contribution and the difference of zero-point vibrational energy (ZPVE) between  $S_1$  and  $S_0$  ( $E_{0-0} = E_{\text{adia}} + \Delta E_{\text{ZPVE}}$ ). Finally, IEF-PCM:TD-DFT single-





point calculations in acetonitrile were performed on the (gas phase) relaxed geometries of  $S_1$ , to evaluate the excited-state dipole moment and photo-induced dipole moment variation  $\Delta\mu_{01}^{\text{opt}^{\pm}}$  accounting for geometrical relaxation effects. All calculations were performed using the Gaussian 09 package.<sup>54</sup>

## Conflicts of interest

The authors declare no conflicts of interest.

## Acknowledgements

MBD gratefully acknowledges the Conseil Régional d'Aquitaine for funding ("Chaire d'Accueil d'excellence" grant). We also acknowledge the University of Bordeaux for fellowships to MK and VD. CT thanks the LAPHIA Centre of Excellence, managed by the ANR under the initiative of excellence (IdEx) program (reference ANR-10-IDEX-0003-02), for her postdoctoral fellowship. Computer time was provided by the Pôle Modélisation HPC facilities of the Institut des Sciences Moléculaires, co-funded by the Nouvelle Aquitaine region.

## Notes and references

- 1 P. Klán, T. Šolomek, C. G. Bochet, A. Blanc, R. Givens, M. Rubina, V. Popik, A. Kostikov and J. Wirz, Photoremovable Protecting Groups in Chemistry and Biology: Reaction Mechanisms and Efficacy, *Chem. Rev.*, 2013, **113**, 119–191.
- 2 G. C. R. Ellis-Davies, Caged compounds: photorelease technology for control of cellular chemistry and physiology, *Nat. Methods*, 2007, **4**, 619–628.
- 3 H. Yu, J. Li, D. Wu, Z. Qiu and Y. Zhang, Chemistry and biological applications of photo-labile organic molecules, *Chem. Soc. Rev.*, 2010, **39**, 464–473.
- 4 R. Horbert, B. Pinchuk, P. Davies, D. Alessi and C. Peifer, Photoactivatable Prodrugs of Antimelanoma Agent Vemurafenib, *ACS Chem. Biol.*, 2015, **10**, 2099–2107.
- 5 D. E. McLain, A. C. Rea, M. B. Widegren and T. M. Dore, Photoactivatable, biologically-relevant phenols with sensitivity toward 2-photon excitation, *Photochem. Photobiol. Sci.*, 2015, **14**, 2151–2158.
- 6 Y. Venkatesh, S. Karthik, Y. Rajesh, M. Mandal, A. Jana and N. D. P. Singh, Three-Arm, Biotin-Tagged Carbazole-Dicyanovinyl-Chlorambucil Conjugate: Simultaneous Tumor Targeting, Sensing, and Photoresponsive Anticancer Drug Delivery, *Chem.-Asian J.*, 2016, **11**, 3482–3486.
- 7 E. M. Callaway and L. C. Katz, Photostimulation using caged glutamate reveals functional circuitry in living brain slices, *Proc. Natl. Acad. Sci. U. S. A.*, 1993, **90**, 7661–7665.
- 8 M. Matsuzaki, G. C. R. Ellis-Davies, T. Nemoto, Y. Miyashita, M. Iino and H. Kasai, Dendritic spine geometry is critical for AMPA receptor expression in hippocampal CA1 pyramidal neurons, *Nat. Neurosci.*, 2001, **4**, 1086–1092.
- 9 T. Furuta, S. S.-H. Wang, J. L. Dantzker, T. M. Dore, W. J. Bybee, E. M. Callaway, W. Denk and R. Y. Tsien, Brominated 7-hydroxycoumarin-4-ylmethyls: Photolabile protecting groups with biologically useful cross-sections for two photon photolysis, *Proc. Natl. Acad. Sci. U. S. A.*, 1999, **96**, 1193–1200.
- 10 F. Terenziani, C. Katan, E. Badaeva, S. Tretiak and M. Blanchard-Desce, Enhanced Two-Photon Absorption of Organic Chromophores: Theoretical and Experimental Assessments, *Adv. Mater.*, 2008, **20**, 4641–4678.
- 11 M. Pawlicki, H. A. Collins, R. G. Denning and H. L. Anderson, Two-Photon Absorption and the Design of Two-Photon Dyes, *Angew. Chem., Int. Ed.*, 2009, **48**, 3244–3266.
- 12 S. Yao and K. D. Belfield, Two-Photon Fluorescent Probes for Bioimaging, *Eur. J. Org. Chem.*, 2012, **2012**, 3199–3217.
- 13 D. Kim, H. G. Ryu and K. H. Ahn, Recent development of two-photon fluorescent probes for bioimaging, *Org. Biomol. Chem.*, 2014, **12**, 4550–4566.
- 14 H. M. Kim and B. R. Cho, Small-Molecule Two-Photon Probes for Bioimaging Applications, *Chem. Rev.*, 2015, **115**, 5014–5055.
- 15 G. Bort, T. Gallavardin, D. Ogden and P. I. Dalko, From One-Photon to Two-Photon Probes: "Caged" Compounds, Actuators, and Photoswitches, *Angew. Chem., Int. Ed.*, 2013, **52**, 4526–4537.
- 16 L. Donato, A. Mourot, C. M. Davenport, C. Herbivo, D. Warther, J. Léonard, F. Bolze, J.-F. Nicoud, R. H. Kramer, M. Goeldner and A. Specht, Water-Soluble, Donor-Acceptor Biphenyl Derivatives in the 2-(*o*-Nitrophenyl)propyl Series: Highly Efficient Two-Photon Uncaging of the Neurotransmitter  $\gamma$ -Aminobutyric Acid at  $\lambda = 800$  nm, *Angew. Chem., Int. Ed.*, 2012, **51**, 1840–1843.
- 17 K. M. Schelkle, T. Griesbaum, D. Ollech, S. Becht, T. Buckup, M. Hamburger and R. Wombacher, Light-Induced Protein Dimerization by One- and Two-Photon Activation of Gibberellic Acid Derivatives in Living Cells, *Angew. Chem., Int. Ed.*, 2015, **54**, 2825–2829.
- 18 Q. Lin, L. Yang, Z. Wang, Y. Hua, D. Zhang, B. Bao, C. Bao, X. Gong and L. Zhu, Coumarin Photocaging Groups Modified with an Electron-Rich Styryl Moiety at the 3-Position: Long-Wavelength Excitation, Rapid Photolysis, and Photobleaching, *Angew. Chem., Int. Ed.*, 2018, **57**, 3722–3726.
- 19 K. A. Korzycka, P. M. Bennett, E. J. Cueto-Diaz, G. Wicks, M. Drobizhev, M. Blanchard-Desce, A. Rebane and H. L. Anderson, Two-photon sensitive protecting groups operating *via* intramolecular electron transfer: uncaging of GABA and tryptophan, *Chem. Sci.*, 2015, **6**, 2419–2426.
- 20 E. Cueto Diaz, S. Picard, M. Klausen, V. Hugues, P. Pagano, E. Genin and M. Blanchard-Desce, Cooperative Veratryle and Nitroindoline Cages for Two-Photon Uncaging in the NIR, *Chem.-Eur. J.*, 2016, **22**, 10848–10859.
- 21 J. P. Olson, H.-B. Kwon, K. T. Takasaki, C. Q. Chiu, M. J. Higley, B. L. Sabatini and G. C. R. Ellis-Davies, Optically Selective Two-Photon Uncaging of Glutamate at 900 nm, *J. Am. Chem. Soc.*, 2013, **135**, 5954–5957.
- 22 J. P. Olson, M. R. Banghart, B. L. Sabatini and G. C. R. Ellis-Davies, Spectral Evolution of a Photochemical Protecting



- Group for Orthogonal Two-Color Uncaging with Visible Light, *J. Am. Chem. Soc.*, 2013, **135**, 15948–15954.
- 23 J. W. Johnson and P. Ascher, Glycine potentiates the NMDA response in cultured mouse brain neurons, *Nature*, 1987, **325**, 529–531.
- 24 R. S. Givens, M. Rubina and J. Wirz, Applications of p-hydroxyphenacyl (pHP) and coumarin-4-ylmethyl photoremovable protecting groups, *Photochem. Photobiol. Sci.*, 2012, **11**, 472–488.
- 25 V. Hagen, B. Dekowski, V. Nache, R. Schmidt, D. Geißler, D. Lorenz, J. Eichhorst, S. Keller, H. Kaneko, K. Benndorf and B. Wiesner, Coumarinylmethyl Esters for Ultrafast Release of High Concentrations of Cyclic Nucleotides upon One- and Two-Photon Photolysis, *Angew. Chem., Int. Ed.*, 2005, **44**, 7887–7891.
- 26 G. P. Hess, B. K. Carpenter, V. Shembekar and Y. Chen, *US Pat.*, 2007243519 (A1), 2007.
- 27 L. Fournier, I. Aujard, T. Le Saux, S. Maurin, S. Beaupierre, J.-B. Baudin and L. Jullien, Coumarinylmethyl Caging Groups with Redshifted Absorption, *Chem.-Eur. J.*, 2013, **19**, 17494–17507.
- 28 Y. Chitose, M. Abe, K. Furukawa and C. Katan, Design, Synthesis, and Reaction of  $\pi$ -Extended Coumarin-based New Caged Compounds with Two-photon Absorption Character in the Near-IR Region, *Chem. Lett.*, 2016, **45**, 1186–1188.
- 29 M.-S. Schiedel, C. A. Briehn and P. Bäuerle, Single-Compound Libraries of Organic Materials: Parallel Synthesis and Screening of Fluorescent Dyes, *Angew. Chem., Int. Ed.*, 2001, **40**, 4677–4680.
- 30 J. Yu and Y. Shirota, A New Class of High-Performance Red-Fluorescent Dyes for Organic Electroluminescent Devices, [7-Diethylamino-3-(2-thienyl)chromen-2-ylidene]-2,2-dicyanovinylamine and {10-(2-Thienyl)-2,3,6,7-tetrahydro-1H,5H-chromeno[8,7,6-ij]quinolizin-11-ylidene}-2,2-dicyanovinylamine, *Chem. Lett.*, 2002, **31**, 984–985.
- 31 A. Gandioso, S. Contreras, I. Melnyk, J. Oliva, S. Nonell, D. Velasco, J. García-Amorós and V. Marchán, Development of Green/Red-Absorbing Chromophores Based on a Coumarin Scaffold That Are Useful as Caging Groups, *J. Org. Chem.*, 2017, **82**, 5398–5408.
- 32 M. Barzoukas and M. Blanchard-Desce, Molecular engineering of push-pull dipolar and quadrupolar molecules for two-photon absorption: A multivalence-bond states approach, *J. Chem. Phys.*, 2000, **113**, 3951–3959.
- 33 K. D. Belfield, A. R. Morales, B.-S. Kang, J. M. Hales, D. J. Hagan, E. W. Van Stryland, V. M. Chapela and J. Percino, Synthesis, Characterization, and Optical Properties of New Two-Photon-Absorbing Fluorene Derivatives, *Chem. Mater.*, 2004, **16**, 4634–4641.
- 34 G. H. Mcgall and A. D. Barone, *US Pat.*, 2011028350 (A1), 2011.
- 35 P. Stegmaier, J. M. Alonso and A. del Campo, Photoresponsive Surfaces with Two Independent Wavelength-Selective Functional Levels, *Langmuir*, 2008, **24**, 11872–11879.
- 36 G. A. Molander and M. R. Rivero, Suzuki Cross-Coupling Reactions of Potassium Alkenyltrifluoroborates, *Org. Lett.*, 2002, **4**, 107–109.
- 37 J. J. Smith, D. Best and H. W. Lam, Copper-catalyzed borylative coupling of vinylazaarenes and N-Boc imines, *Chem. Commun.*, 2016, **52**, 3770–3772.
- 38 T. Jeffery, On the efficiency of tetraalkylammonium salts in Heck type reactions, *Tetrahedron*, 1996, **52**, 10113–10130.
- 39 C. Bao, G. Fan, Q. Lin, B. Li, S. Cheng, Q. Huang and L. Zhu, Styryl Conjugated Coumarin Caged Alcohol: Efficient Photorelease by Either One-Photon Long Wavelength or Two-Photon NIR Excitation, *Org. Lett.*, 2012, **14**, 572–575.
- 40 M. Petit, C. Tran, T. Roger, T. Gallavardin, H. Dhimane, F. Palma-Cerda, M. Blanchard-Desce, F. C. Acher, D. Ogden and P. I. Dalko, Substitution Effect on the One- and Two-photon Sensitivity of DMAQ “Caging” Groups, *Org. Lett.*, 2012, **14**, 6366–6369.
- 41 S. Picard, E. Genin, G. Clermont, V. Hugues, O. Mongin and M. Blanchard-Desce, Octupolar chimeric compounds built from quinoline caged acetate moieties: a novel approach for 2-photon uncaging of biomolecules, *New J. Chem.*, 2013, **37**, 3899–3913.
- 42 S. R. Adams, J. P. Y. Kao, G. Grynkiewicz, A. Minta and R. Y. Tsien, Biologically useful chelators that release  $\text{Ca}^{2+}$  upon illumination, *J. Am. Chem. Soc.*, 1988, **110**, 3212–3220.
- 43 T. Šolomek, J. Wirz and P. Klán, Searching for Improved Photoreleasing Abilities of Organic Molecules, *Acc. Chem. Res.*, 2015, **48**, 3064–3072.
- 44 Y. Zhao and D. G. Truhlar, The M06 suite of density functionals for main group thermochemistry, thermochemical kinetics, noncovalent interactions, excited states, and transition elements: two new functionals and systematic testing of four M06-class functionals and 12 other functionals, *Theor. Chem. Acc.*, 2008, **120**, 215–241.
- 45 B. Schade, V. Hagen, R. Schmidt, R. Herbrich, E. Krause, T. Eckardt and J. Bendig, Deactivation Behavior and Excited-State Properties of (Coumarin-4-yl)methyl Derivatives. 1. Photocleavage of (7-Methoxycoumarin-4-yl)methyl-Caged Acids with Fluorescence Enhancement, *J. Org. Chem.*, 1999, **64**, 9109–9117.
- 46 R. Schmidt, D. Geissler, V. Hagen and J. Bendig, Kinetics Study of the Photocleavage of (Coumarin-4-yl)methyl Esters, *J. Phys. Chem. A*, 2005, **109**, 5000–5004.
- 47 A. Fischer, C. Cremer and E. H. K. Stelzer, Fluorescence of coumarins and xanthenes after two-photon absorption with a pulsed titanium-sapphire laser, *Appl. Opt.*, 1995, **34**, 1989–2003.
- 48 F. Terenziani, M. Morone, S. Gmouh and M. Blanchard-Desce, Linear and Two-Photon Absorption Properties of Interacting Polar Chromophores: Standard and Unconventional Effects, *ChemPhysChem*, 2006, **7**, 685–696.
- 49 A. S. Melnikov, P. Y. Serdobintsev, A. D. Vedyaykin and M. A. Khodorkovskii, Two-photon absorption cross section for Coumarins 102, 153 and 307, *J. Phys.: Conf. Ser.*, 2017, **917**, 062029.
- 50 The extrapolated  $\delta_{\text{u}}$  value for DEAC450, determined from measurements conducted in MeCN/H<sub>2</sub>O (90/10, v/v) is two



orders larger than the one reported in the literature for direct  $\delta_u$  measurements conducted in biological medium. Although the 2PA response of **DEAC450** was found to depend on the solvent (see ESI†), this could not account for such a discrepancy. Our study suggests that the reported  $\delta_u$  value for **DEAC450** may be significantly underestimated, making it one of the best 2P uncagers currently available.

- 51 J. Tomasi, B. Mennucci and R. Cammi, Quantum Mechanical Continuum Solvation Models, *Chem. Rev.*, 2005, **105**, 2999–3094.
- 52 T. Le Bahers, C. Adamo and I. Ciofini, A Qualitative Index of Spatial Extent in Charge-Transfer Excitations, *J. Chem. Theory Comput.*, 2011, **7**, 2498–2506.
- 53 D. Jacquemin, T. L. Bahers, C. Adamo and I. Ciofini, What is the “best” atomic charge model to describe through-space charge-transfer excitations?, *Phys. Chem. Chem. Phys.*, 2012, **14**, 5383–5388.
- 54 M. J. Frisch, G. W. Trucks, H. B. Schlegel, G. E. Scuseria, M. A. Robb, J. R. Cheeseman, G. Scalmani, V. Barone, B. Mennucci, G. A. Petersson, H. Nakatsuji, M. Caricato, X. Li, H. P. Hratchian, A. F. Izmaylov, J. Bloino, G. Zheng, J. L. Sonnenberg, M. Hada, M. Ehara, K. Toyota, R. Fukuda, J. Hasegawa, M. Ishida, T. Nakajima, Y. Honda, O. Kitao, H. Nakai, T. Vreven, J. A. Montgomery Jr, J. E. Peralta, F. Ogliaro, M. Bearpark, J. J. Heyd, E. Brothers, K. N. Kudin, V. N. Staroverov, R. Kobayashi, J. Normand, K. Raghavachari, A. Rendell, J. C. Burant, S. S. Iyengar, J. Tomasi, M. Cossi, C. Rega, J. M. Millam, M. Klene, J. E. Knox, J. B. Cross, V. Bakken, C. Adamo, J. Jaramillo, R. Gomperts, R. E. Stratmann, O. Yazyev, A. J. Austin, R. Cammi, C. Pomelli, J. W. Ochterski, R. L. Martin, K. Morokuma, V. G. Zakrzewski, G. A. Voth, P. Salvador, J. J. Dannenberg, S. Dapprich, A. D. Daniels, Ö. Farkas, J. B. Foresman, J. V. Ortiz, J. Cioslowski and D. J. Fox, *Gaussian 09 revision D01*, Gaussian Inc., Wallingford CT, 2009.

